

## Isomers in $^{203}\text{Tl}$ and core excitations built on a five-nucleon-hole structure

V. Bothe <sup>1,\*</sup> S. K. Tandel <sup>1,2,†</sup> S. G. Wahid <sup>1,‡</sup> P. C. Srivastava <sup>3</sup> Bharti Bhoj <sup>3</sup> P. Chowdhury,<sup>2</sup>  
R. V. F. Janssens <sup>4,5</sup> F. G. Kondev <sup>6</sup> M. P. Carpenter,<sup>6</sup> T. Lauritsen <sup>6</sup> D. Seweryniak,<sup>6</sup> and S. Zhu<sup>6,§</sup>

<sup>1</sup>*School of Physical Sciences, UM-DAE Centre for Excellence in Basic Sciences, Mumbai 400098, India*

<sup>2</sup>*Department of Physics, University of Massachusetts Lowell, Lowell, Massachusetts 01854, USA*

<sup>3</sup>*Department of Physics, Indian Institute of Technology Roorkee, Roorkee 247667, India*

<sup>4</sup>*Department of Physics and Astronomy, University of North Carolina at Chapel Hill, Chapel Hill, North Carolina 27599, USA*

<sup>5</sup>*Triangle Universities Nuclear Laboratory, Duke University, Durham, North Carolina 27708, USA*

<sup>6</sup>*Argonne National Laboratory, Argonne, Illinois 60439, USA*



(Received 3 June 2021; revised 18 October 2021; accepted 15 April 2022; published 27 April 2022)

Isomers with three- and five-nucleon-hole configurations have been established in  $^{203}\text{Tl}$ . These include newly identified levels with a three-nucleon-hole structure:  $I^\pi = (15/2^-)$  with  $T_{1/2} = 7.9(5)$  ns and  $I^\pi = (35/2^-)$  with  $T_{1/2} = 4.0(5)$  ns. In addition, five-nucleon-hole states have also been established:  $I^\pi = (39/2^-)$  with  $T_{1/2} = 1.9(2)$  ns and  $I^\pi = (49/2^+)$  with  $T_{1/2} = 3.4(4)$  ns. The previously determined long-lived decay,  $T_{1/2} = 6.6(3)$   $\mu\text{s}$  from this work, is associated with isomerism of the  $I^\pi = (29/2^+)$  state. Levels above this long-lived isomer have been identified through a delayed-prompt  $\gamma - \gamma$  coincidence measurement. Five-nucleon-hole states with excitation energies  $E_x \approx 7$  MeV have been established as well as possible octupole excitations of the  $^{208}\text{Pb}$  core built on these levels. The level scheme of  $^{203}\text{Tl}$  is extended up to  $E_x \approx 11$  MeV with the inclusion of 25 new transitions. Empirical and shell-model calculations have been performed to aid in the description of the observed states which are found to be of intrinsic character.

DOI: [10.1103/PhysRevC.105.044327](https://doi.org/10.1103/PhysRevC.105.044327)

### I. INTRODUCTION

The occurrence of metastable states in nuclei with proton or neutron numbers in the vicinity of shell closures is well established as arising from the presence of adjacent excited levels with a relatively large difference in angular momentum and small difference in energy. Isotopes of Hg ( $Z = 80$ ) and Tl ( $Z = 81$ ) with  $A \approx 200$ , lying just below the doubly magic  $^{208}\text{Pb}$  nucleus in the periodic chart, are therefore good candidates for the observation of metastable states or isomers [1–5]. The lighter isotopes of Tl ( $A < 200$ ) are characterized by moderate oblate deformation on account of a significant number of valence neutrons leading to a small degree of collectivity [6,7]. However, when approaching the  $N = 126$  shell gap, collective behavior is no longer evident. This is the case for isotopes of Tl near the line of stability, where  $^{203}\text{Tl}$  and  $^{205}\text{Tl}$  are the two stable isotopes [1–3,8,9]. The nucleus  $^{203}\text{Tl}$ , with  $N = 122$ , is only one proton and four neutron holes away from doubly magic  $^{208}\text{Pb}$  and, as a result, its structure is expected to be dominated by single-particle excitations. The

available valence orbitals are the proton  $s_{1/2}$ ,  $d_{3/2}$ ,  $d_{5/2}$ , and  $h_{11/2}$  states and the neutron  $p_{1/2}$ ,  $p_{3/2}$ ,  $f_{5/2}$ , and  $i_{13/2}$  ones. The presence of the unique-parity  $\pi h_{11/2}$  and  $\nu i_{13/2}$  orbitals allows for the realization of yrast, high-spin states, some of which may be of isomeric character, owing to hindrance induced by the angular momentum selection rule or a change in configuration.

The systematic delineation of isomers along an isotopic chain, most of which have relatively pure intrinsic character, provides a host of nuclear structure information, among which figure residual interactions between nucleons occupying different subshells. Heavy-ion and  $\alpha$ -induced reactions have been used to populate excited states at high spin in lighter Tl isotopes [7,10]. However, in order to study isotopes near the line of stability, different reaction mechanisms such as inelastic excitation and multinucleon transfer may be utilized. In order to populate states with high spin, heavy projectiles with above-barrier energies are required. The isotopes of Tl approaching the shell closure at  $N = 126$ , particularly  $^{204,205}\text{Tl}$  [2,3], have been studied up to high spin and several metastable states established. In contrast, there was limited knowledge on isomers in  $^{200-203}\text{Tl}$  prior to investigations by this collaboration. Recently, the observation of isomers with half-lives ranging from a few nanoseconds to hundreds of microseconds in  $^{200}\text{Tl}$  [11] and  $^{202}\text{Tl}$  [8] were reported. The existing information on  $^{203}\text{Tl}$  prior to the present work is limited, with levels up to possible spin  $(17/2) \hbar$  and excitation energy  $\approx 3$  MeV established through a deuteron-induced reaction [9], while a microsecond isomer was identified using

\*Present address: Max-Planck-Institut für Kernphysik, Postfach 103980, 69029 Heidelberg, Germany.

†Corresponding author: [sujit.tandel@cbs.ac.in](mailto:sujit.tandel@cbs.ac.in); [sktandel@gmail.com](mailto:sktandel@gmail.com).

‡Present address: University of Massachusetts Lowell, Lowell, Massachusetts 01854, USA.

§Deceased.

projectile fragmentation [12]. In the former instance, the presence of a nanosecond isomer has been inferred, but its location was not established. In the latter case, no level scheme is reported, and a tentative assignment of  $I^\pi = (25/2^+)$  and a three-nucleon-hole character for the microsecond isomer was proposed. Projectile-fragmentation reactions have been utilized to identify and study isomers in a number of neutron-rich isotopes like  $^{204}\text{Pt}$ ,  $^{205}\text{Au}$ , and many in the Ta-Hg and Pt-Rn regions, including several even- $A$  Pb nuclei [13–17]. The motivation for the present work was to obtain unambiguous information on the structural aspects mentioned above in order to advance the understanding of the structure of  $^{203}\text{Tl}$ . An additional goal was to extend the level scheme of  $^{203}\text{Tl}$  to also encompass levels arising from the maximum possible number of nucleon-hole excitations, which is five in this case, which allows for discriminating tests of interactions used in shell-model calculations. Furthermore, it was also proposed to investigate the presence of possible octupole core excitations in  $^{203}\text{Tl}$  which would be built on five-nucleon-hole configurations. In this region, such excitations have thus far been observed only in  $^{203}\text{Hg}$  [4].

## II. EXPERIMENT AND DATA ANALYSIS

Multinucleon transfer reactions were used to populate excited states in  $^{203}\text{Tl}$ , with a 1450-MeV  $^{209}\text{Bi}$  beam from the ATLAS accelerator at Argonne National Laboratory, incident on a thick, 50-mg/cm<sup>2</sup> Au target. The  $\gamma$ -ray coincidence data were recorded with the Gammasphere array comprised of 100 Compton-suppressed high-purity germanium detectors at the time of the experiment [18,19]. In addition to “prompt” coincidence events, “delayed” data from the decay of isomeric levels were also recorded. The terms “prompt” and “delayed” refer to  $\gamma$  rays recorded within  $\approx 40$  ns of the beam being incident on the target, and those detected after this duration, respectively. In the first instance, the  $^{209}\text{Bi}$  beam, with the usual 82.5 ns pulsing from the ATLAS superconducting linear accelerator, was incident on the target for a few ns and then swept away for a 825-ns off period. Three- and higher-fold coincidence events were recorded within a 1- $\mu\text{s}$  coincidence window, allowing for the measurement of half-lives ranging from a few to several hundred nanoseconds. Later, two- and higher-fold coincidence data were collected only during beam-off periods by sweeping the beam with an ON/OFF ratio of 200  $\mu\text{s}$ /800  $\mu\text{s}$  via a free-running external clock, enabling the study of isomers with long ( $\mu\text{s}$ ) half-lives.

The coincidence data were sorted into a variety of histograms in order to establish the level structure and determine the half-lives of isomers using the TSCAN [20] and Radware [21] suite of programs. Three-dimensional histograms of prompt and delayed coincidence events were created and analyzed, corresponding to the detection of at least three  $\gamma$  rays within  $\pm 40$  ns and 50–650 ns of the trigger, respectively. To identify  $\gamma$  rays feeding the  $\mu\text{s}$  isomer, a three-dimensional histogram requiring two delayed  $\gamma$ -ray events together with a prompt one, was constructed. The centroid-shift method was used to determine half-lives ranging between  $\approx 1$  and 10 ns using an energy-gated two-dimensional histogram with energy on one axis and time difference of the associated  $\gamma$

rays on the other. The coincidence relationships between  $\gamma$  rays deexciting the  $\mu\text{s}$  isomer were also analyzed with the help of a three-dimensional energy histogram consisting of events detected in the 800- $\mu\text{s}$  beam-off period. To determine the half-life of the  $\mu\text{s}$  isomer, several three-dimensional histograms spanning suitable time intervals within the 800- $\mu\text{s}$  beam-off period were created.

Multipolarity assignments for some of the transitions below the long-lived ( $\mu\text{s}$ ) isomer in  $^{203}\text{Tl}$  have been obtained using intensity balance considerations. The total intensities feeding and deexciting a given level populated in the delayed data from the decay of the  $\mu\text{s}$  isomer have been considered. Theoretical values of conversion coefficients [22] have been used. For relatively high-energy transitions ( $> 600$  keV), the choice of multipolarity does not significantly affect the value of the total intensity inferred from the  $\gamma$ -ray intensity. For lower-energy, less-intense transitions, the choice of multipolarity does not significantly affect the sum of intensities feeding or deexciting a given level. This procedure has been used to assign multipolarity to transitions with relatively low energy ( $\approx 100$ – $400$  keV), which may have significant conversion coefficients. Further details of the above data analysis methods are described elsewhere [8,11,23–25]. It may be noted that Tl x rays are not clearly visible in the spectra since Pb absorbers were placed on the Ge-detector modules to prevent triggering on x rays primarily from the excitation of the Au target.

The relative intensities of  $\gamma$  rays above the  $\mu\text{s}$  isomer have been obtained as follows. The most intense  $\gamma$  rays feeding the isomer were identified through an inspection of delayed-prompt  $\gamma$ -ray data by requiring coincidences with transitions deexciting the isomer. A few of the most intense  $\gamma$  rays were thus placed above the  $\mu\text{s}$  isomer. The subsequent placements were done by gating on these newly identified  $\gamma$  rays in the prompt data and inspecting the observed coincident transitions and their  $\gamma$ -ray intensities. Multipolarities of the low-energy transitions were determined from intensity balance considerations after gating on the newly observed, higher-lying, 2306-keV line, combined with theoretical conversion coefficients [22], as described earlier.

## III. RESULTS

Excited states in  $^{203}\text{Tl}$  up to medium spin and excitation energy of  $E_x \approx 3$  MeV had been identified earlier through the  $^{204}\text{Hg}(d, 3n)$  reaction with an incident deuteron energy of  $\approx 25$  MeV [9], and projectile fragmentation using a 1-GeV/nucleon  $^{238}\text{U}$  beam on a thick  $^9\text{Be}$  target [12]. In the former, a cascade of  $\gamma$  rays with transition energies of 588, 533, 328, 350, and 265 keV were placed, in that order, above the  $11/2^-$  level at 1450 keV. The presence of an isomer with  $T_{1/2} = 7.9_{-13}^{+10}$  ns had been inferred; however, its precise location had not been determined. From the projectile fragmentation work, feeding from a long-lived,  $T_{1/2} = 7.7(5)$   $\mu\text{s}$  isomer was reported and a spin-parity,  $I^\pi = (25/2^+)$ , was suggested. Though the above  $\gamma$  rays were observed, a level scheme was not reported.

The level scheme for  $^{203}\text{Tl}$  deduced from the present work is shown in Fig. 1. The presence of the two previously

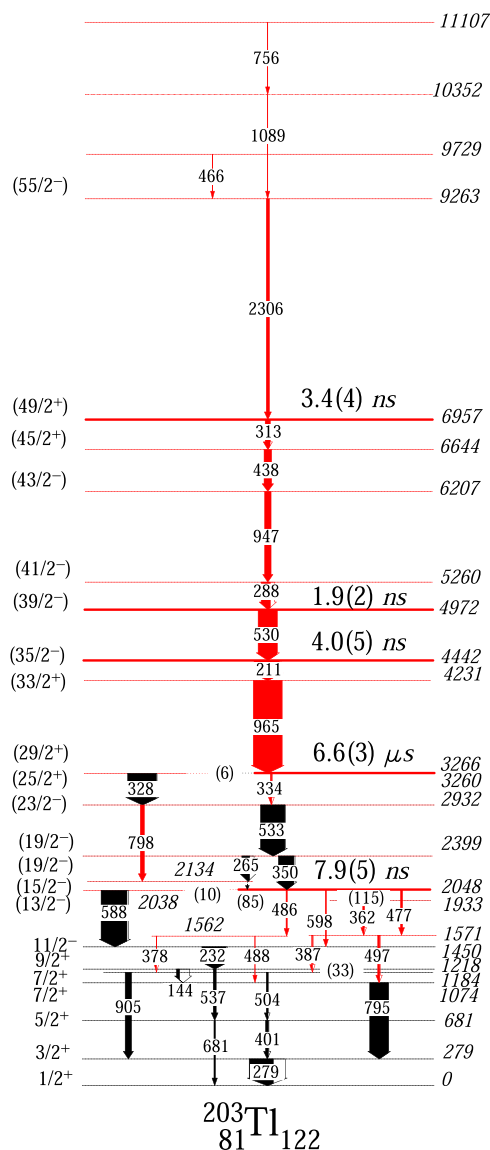


FIG. 1. Partial level scheme of  $^{203}\text{Tl}$  obtained from the present work. The transitions and levels above the  $(29/2^+)$  isomeric state at 3266 keV, and several below it (marked in red), are newly established. All energies are in keV. Measured half-lives are listed above the respective levels *viz.* the  $(15/2^-)$ ,  $(29/2^+)$ ,  $(35/2^-)$ ,  $(39/2^-)$ , and  $(49/2^+)$  isomers. The filled (open) parts of the arrows indicate  $\gamma$  ray (internal conversion) intensities.

reported isomers is confirmed, and a slightly improved value of half-life is deduced for the  $\mu\text{s}$  isomer. The placements of the previously reported  $\gamma$  rays and level energies above the 588-keV,  $13/2^- \rightarrow 11/2^-$  transition, have been revised as described below, based on observed  $\gamma$  rays and their coincidence relationships in the three-dimensional energy histogram. A new level with  $E_x = 2048$  keV and possible spin-parity  $I^\pi = (15/2^-)$  is established. Several decay branches are observed from this state, including the 598-, 486-, and 477-keV  $\gamma$  rays, along with an unobserved 10-keV transition to the  $I^\pi = 13/2^-$  level. From previous work [9,12], the 350- and 265-keV  $\gamma$  rays were inferred to be in cascade above the 328-

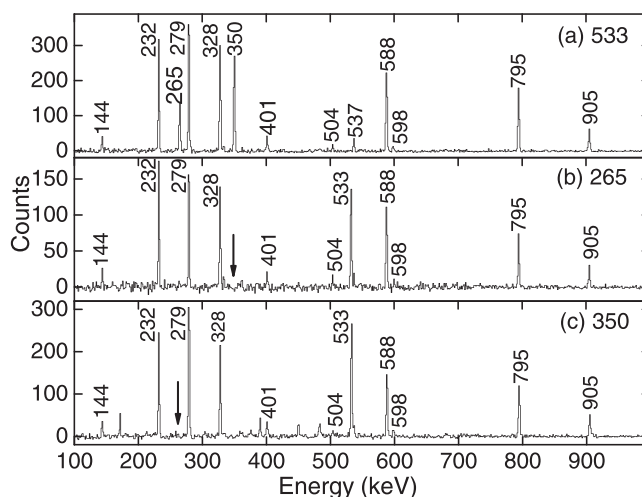


FIG. 2. Summed spectra in coincidence with two  $\gamma$  rays illustrating coincidence relationships with the (a) 533-, (b) 265-, (c) 350-keV transitions, together with any of the 232-, 328-, and 588-keV transitions. It is evident that the 265- and 350-keV transitions, the positions of which are marked with arrows in the middle and lower panels, are not coincident with each other as previously proposed [9,12]. The binning is 1.33 keV/channel.

and 533-keV transitions. The present data unambiguously indicate that these 350- and 265-keV  $\gamma$  rays are not in mutual coincidence although they are coincident with all lower- and higher-lying transitions, as illustrated in Fig. 2. The presence of an unobserved 85-keV transition in cascade with the 265-keV line, but not with the 350-keV transition, was ascertained. One key evidence leading to the revised placements was the observation of a weak 798-keV  $\gamma$  ray which is found to be coincident with the 328-keV and all lower-lying transitions, but not with the 533-, 350-, and 265-keV ones, as shown in Fig. 3. Another crucial indicator is the observation of a weak

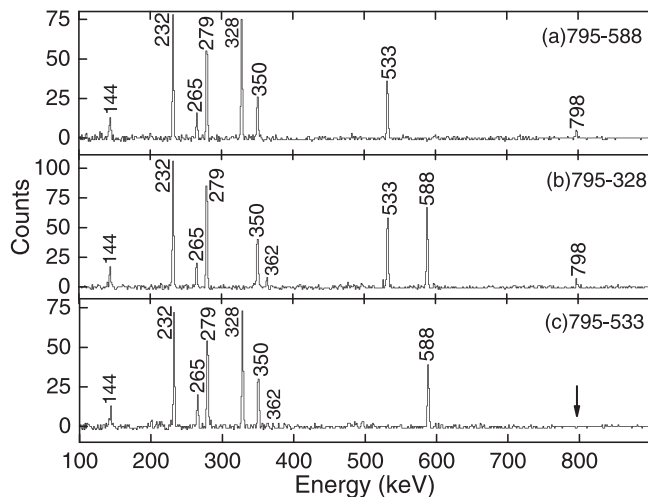


FIG. 3. Summed spectra in coincidence with two  $\gamma$  rays indicated in the panels, illustrating that the newly observed 798-keV  $\gamma$  ray is coincident with the 588- and 328-keV transitions, but not with the 533-keV one (arrow). The binning is 1.33 keV/channel.

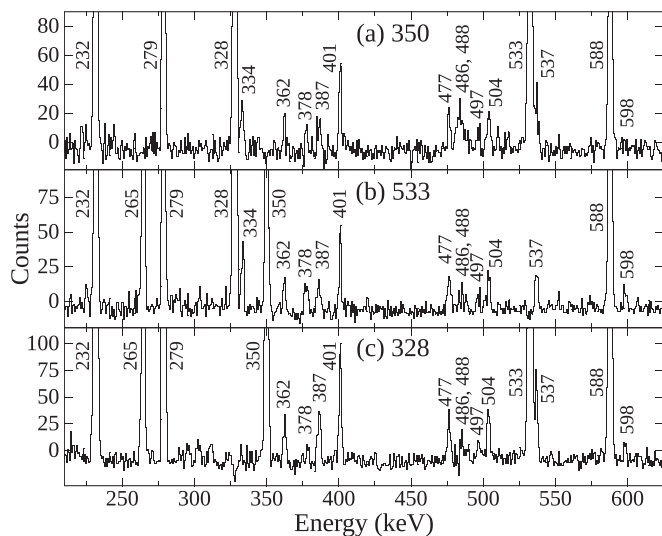


FIG. 4. Summed spectra in coincidence with two  $\gamma$  rays, with the common one indicated in the panels, highlighting the presence of the 334-keV isomeric transition in the 350- and 533-keV gated spectra, and its absence in the 328-keV gated spectrum. The newly observed, less-intense  $\gamma$  rays are also clearly visible. The binning is 1.33 keV/channel.

334-keV transition in coincidence with all  $\gamma$  rays except with the 328-keV one (see Fig. 4). The 334-keV transition is clearly visible in the delayed spectra but not in the prompt ones. These coincidence relationships, along with intensity balance arguments from the delayed data, justify the revision in the relative placement of the transitions. Further, inspection of the prompt spectra reveals that the intensity of the transitions reduces approaching the  $(29/2^+)$  isomer at 3266 keV, in the order 588, 350, 533, and 328 keV, respectively. The 334- and 798-keV  $\gamma$  rays may not have been identified in the previous work on account of their low intensity and proximity of the 798-keV  $\gamma$  ray to the intense,  $7/2^+ \rightarrow 3/2^+$ , 795-keV transition. The newly determined levels above the  $E_x = 2048$ -keV state are, therefore, the ones with  $E_x = 2134$ , 2399, 2932, 3260, and 3266 keV and  $I^\pi = (19/2^-)$ ,  $(19/2^-)$ ,  $(23/2^-)$ ,  $(25/2^+)$ , and  $(29/2^+)$ , respectively (Fig. 1). The 328-keV  $\gamma$  ray deexciting the 3260-keV level is assigned probable  $E1$  character from intensity balance considerations, as determined in the delayed spectra, with the  $3/2^+ \rightarrow 1/2^+$ , 279-keV transition, using its measured conversion coefficient [26], and the  $5/2^+ \rightarrow 1/2^+$ , 681-keV  $\gamma$  ray, as described below. As stated above, the presence of an unobserved, 85-keV transition linking the 2134- and 2048-keV levels is inferred. For the isomeric, 334-keV  $\gamma$  ray, a  $(29/2^+) \rightarrow (23/2^-)$ ,  $E3$  assignment appears to be implied, also described below. The presence of an unobserved 6-keV,  $(29/2^+) \rightarrow (25/2^+)$ ,  $E2$  transition, also deexciting the isomer is inferred. A few of the less intense  $\gamma$  rays which are placed in the level scheme are clearly visible in the summed coincidence spectra in Fig. 4. The  $\gamma$  rays observed following the deexcitation of the  $I^\pi = (29/2^+)$  isomer at 3266 keV are listed in Table I.

An illustrative example of multipolarity assignments using the intensity-balance method for the 328- and 334-keV

transitions is given below. In the delayed spectra, the summed total intensity of the 279- and 681-keV transitions mentioned above should be balanced with the sum of the total intensities of the 328- and 334-keV transitions deexciting the  $(25/2^+)$  and  $(29/2^+)$  levels, respectively (Fig. 1). The conversion coefficient of the 279-keV transition is measured to be 0.2261(9) [27] and the theoretical value of the same for the 681-keV transition is 0.014 [22]. Using the measured  $\gamma$ -ray intensities, the summed total intensity of the 279- and 681-keV transitions is found to be 108(5). This value has to be balanced with the summed total intensity of the 328- and 334-keV transitions, allowing for all physically reasonable combinations of multiplicities, along with the inclusion of constraints provided by the data. The inferred summed total intensity of the 328- and 334-keV transitions using their measured  $\gamma$ -ray intensities (Table I) and theoretical conversion coefficients are (a) 328 ( $E1$ ) and 334 ( $E3$ ): 107(5); (b) 328 ( $M1$ ) and 334 ( $E3$ ): 136(7); and (c) 328 ( $E2$ ) and 334 ( $E3$ ): 114(5). Other possible combinations, involving a different multipolarity for either of the two transitions, are quite unlikely based on the data. Therefore,  $E1$  and  $E3$  character, respectively, are inferred for the 328- and 334-keV transitions, since in this case, their summed total intensity best matches that of the combined value of the 279- and 681-keV transitions. Similar considerations lead to the determination of probable  $E2$  and  $M1 + E2$  character for the 350- and 265-keV transitions. It may be noted that, while intensity balance considerations do not rule out  $E2$  multipolarity for the 328-keV transition, in comparison to the proposed  $E1$  character, the  $E2$  assignment for the 328-keV  $\gamma$  ray would imply  $E1$  nature for the most intense, 6-keV decay branch from the 6.6- $\mu$ s isomer, which is quite unlikely. Therefore, the 328-keV transition is assigned  $E1$  multipolarity.

The  $I^\pi = (15/2^-)$  state at  $E_x = 2048$  keV is determined to be isomeric with  $T_{1/2} = 7.9(5)$  ns, in agreement with the previously reported value [9]. The histogram of time difference of  $\gamma$  rays below and above this state and a comparison with prompt transitions of similar energy can be found in Fig. 5. The level at  $E_x = 2048$  keV, which is assigned  $I^\pi = (15/2^-)$  decays by an unobserved 10-keV transition to the 2038-keV level with  $I = (13/2)$  reported earlier [9]. Apart from other transitions which deexcite this state, a 598-keV  $\gamma$  ray is observed to decay to the  $11/2^-$  level at 1450 keV. The total intensity of the 10-keV branch is much greater than that of the 598-keV one as evidenced by a comparison of the  $\gamma$ -ray intensities of the 588-keV (in cascade with 10 keV) and the 598-keV lines. It is unlikely that out of two transitions with hypothetically the same multipolarity, the one with the much lower energy would be, by far, the more intense branch. Therefore, the 10- and 598-keV transitions are assigned  $M1$  and  $E2$  multipolarity, respectively, leading to the  $(15/2^-)$  assignment for the 2048-keV level. Additionally, the data indicate the possibility of isomerism of the 2134-keV level, with a half-life up to several nanoseconds; however, the low intensity and energy of the transitions involved do not allow for a measurement of its value. All  $\gamma$  rays below the  $(29/2^+)$  state at 3266 keV are found to exhibit delayed feeding in the 800- $\mu$ s beam-off period. The integral variation in intensity with time of summed coincidence counts, with gates on the

TABLE I. Energies and intensities of  $\gamma$  rays and excitation energies and spins of initial and final states in  $^{203}\text{Tl}$  up to the 6.6- $\mu\text{s}$  isomer. Statistical uncertainties on  $\gamma$ -ray energies and intensities are listed. Relative intensities have been obtained from delayed data (between 50 and 650 ns of the beam being incident on the target). Theoretical values of total conversion coefficients ( $\alpha$ ) for the listed multipolarities from the BRICC tabulation [22] are listed where required. Probable predominant multipolarities determined from intensity balance considerations are noted in parentheses for selected transitions.

$E_\gamma$ (keV)	$E_i$ (keV) $\rightarrow$ $E_f$ (keV)	$I_i^\pi \rightarrow I_f^\pi$	$I_\gamma$	$\alpha$	Mult.
(6)	3265.5 $\rightarrow$ 3259.9	(29/2 <sup>+</sup> ) $\rightarrow$ (25/2 <sup>+</sup> )	–		
(10)	2048.4 $\rightarrow$ 2038.3	(15/2 <sup>-</sup> ) $\rightarrow$ (13/2 <sup>-</sup> )	–		
(33)	1217.9 $\rightarrow$ 1184.4	9/2 <sup>+</sup> $\rightarrow$ 7/2 <sup>+</sup>	–		
(85)	2133.7 $\rightarrow$ 2048.4	(19/2 <sup>-</sup> ) $\rightarrow$ (15/2 <sup>-</sup> )	–		
(115)	2048.4 $\rightarrow$ 1933.3	(15/2 <sup>-</sup> ) $\rightarrow$ –	–		
143.5(2)	1217.9 $\rightarrow$ 1074.3	9/2 <sup>+</sup> $\rightarrow$ 7/2 <sup>+</sup>	11(3)		
232.0(1)	1449.9 $\rightarrow$ 1217.9	11/2 <sup>-</sup> $\rightarrow$ 9/2 <sup>+</sup>	84(5)		
265.0(1)	2398.7 $\rightarrow$ 2133.7	(19/2 <sup>-</sup> ) $\rightarrow$ (19/2 <sup>-</sup> )	27(3)		(M1 + E2)
279.3(1)	279.3 $\rightarrow$ 0.0	3/2 <sup>+</sup> $\rightarrow$ 1/2 <sup>+</sup>	84(4)		
328.1(1)	3259.9 $\rightarrow$ 2931.8	(25/2 <sup>+</sup> ) $\rightarrow$ (23/2 <sup>-</sup> )	100(5)	0.023	(E1)
333.7(3)	3265.5 $\rightarrow$ 2931.8	(29/2 <sup>+</sup> ) $\rightarrow$ (23/2 <sup>-</sup> )	4(1)	0.385	(E3)
350.3(1)	2398.7 $\rightarrow$ 2048.4	(19/2 <sup>-</sup> ) $\rightarrow$ (15/2 <sup>-</sup> )	54(4)	0.071	(E2)
362.1(2)	1933.3 $\rightarrow$ 1571.2	– $\rightarrow$ –	3(1)		
378.3(4)	1562.3 $\rightarrow$ 1184.4	– $\rightarrow$ 7/2 <sup>+</sup>	<2		
387.1(5)	1571.2 $\rightarrow$ 1184.4	– $\rightarrow$ 7/2 <sup>+</sup>	3(1)		
401.4(2)	680.7 $\rightarrow$ 279.3	5/2 <sup>+</sup> $\rightarrow$ 3/2 <sup>+</sup>	10(2)		
477.3(2)	2048.4 $\rightarrow$ 1571.2	(15/2 <sup>-</sup> ) $\rightarrow$ –	7(2)		
485.8(4)	2048.4 $\rightarrow$ 1562.3	(15/2 <sup>-</sup> ) $\rightarrow$ –	4(1)		
488.2(4)	1562.3 $\rightarrow$ 1074.3	– $\rightarrow$ 7/2 <sup>+</sup>	<2		
496.9(3)	1571.2 $\rightarrow$ 1074.3	– $\rightarrow$ 7/2 <sup>+</sup>	7(2)		
503.9(2)	1184.4 $\rightarrow$ 680.7	7/2 <sup>+</sup> $\rightarrow$ 5/2 <sup>+</sup>	6(1)		
533.1(1)	2931.8 $\rightarrow$ 2398.7	(23/2 <sup>-</sup> ) $\rightarrow$ (19/2 <sup>-</sup> )	85(6)	0.024	(E2)
537.3(2)	1217.9 $\rightarrow$ 680.7	9/2 <sup>+</sup> $\rightarrow$ 5/2 <sup>+</sup>	10(2)		
588.4(1)	2038.3 $\rightarrow$ 1449.9	(13/2 <sup>-</sup> ) $\rightarrow$ 11/2 <sup>-</sup>	90(6)		
598.5(3)	2048.4 $\rightarrow$ 1449.9	(15/2 <sup>-</sup> ) $\rightarrow$ 11/2 <sup>-</sup>	4(1)		
680.6(3)	680.7 $\rightarrow$ 0	5/2 <sup>+</sup> $\rightarrow$ 1/2 <sup>+</sup>	5(1)		
795.0(1)	1074.3 $\rightarrow$ 279.3	7/2 <sup>+</sup> $\rightarrow$ 3/2 <sup>+</sup>	65(5)		
797.6(3)	2931.8 $\rightarrow$ 2133.7	(23/2 <sup>-</sup> ) $\rightarrow$ (19/2 <sup>-</sup> )	14(3)		
905.1(2)	1184.4 $\rightarrow$ 279.3	7/2 <sup>+</sup> $\rightarrow$ 3/2 <sup>+</sup>	22(3)		

232-, 265-, 279-, 328-, 533-, 588-, and 795-keV  $\gamma$  rays is illustrated in Fig. 6. A value of  $T_{1/2} = 6.6(3) \mu\text{s}$  is obtained, with an uncertainty that is slightly below the quoted one in the previous work, i.e.,  $7.7(5) \mu\text{s}$  [12]. The measured value is associated with the half-life of the  $I^\pi = (29/2^+)$  state.

Typically, the presence of an intervening long-lived (approximately  $\mu\text{s}$  or greater) isomer prevents the identification of  $\gamma$  rays feeding such a level. In this case, with the 1- $\mu\text{s}$  Gammasphere coincidence window and the 6.6(3)- $\mu\text{s}$  half-life, only a small number of coincidence events comprising  $\gamma$  rays below and above the isomer were recorded. By summing spectra measured in coincidence with two intense delayed transitions below the isomer in a three-dimensional histogram, several prompt  $\gamma$  rays feeding the isomer could be identified [Fig. 7(a)]. The following  $\gamma$  rays were found to be in coincidence with the delayed transitions as well as with each other: 965, 211, 530, 288, 947, 438, and 313 keV. While their ordering has been obtained using the methods described earlier, in specific instances like the 211- and 530-keV  $\gamma$  rays, where the intensities are similar (within uncertainties), the isomeric character of the 4442-keV state allows for determining their order, i.e., the 211-keV  $\gamma$  ray is on average detected later than

the 530-keV one. Detailed information on these transitions is presented in Fig. 1 and Table II. Though some random contaminant transitions are also present in Fig. 7(a), their origin was accounted for in terms of the deexcitation of low-lying states from the strong reaction channels observed in the data. The spin-parity assignments of the levels above the (29/2<sup>+</sup>) state are based on both experimental data and systematics [28] as described below and should be considered tentative. Figure 7(b) is the spectrum in prompt coincidence with gates on the 530- and 965-keV transitions. Additionally, four other significantly weaker  $\gamma$  rays, with energies 466, 756, 1089, and 2306 keV, were also visible in prompt coincidence and are found to be enhanced in the summed prompt coincidence spectrum with gates on transitions between the (29/2<sup>+</sup>) and the 6957-keV, (49/2<sup>+</sup>) levels [Fig. 7(c)]. The 2306-keV  $\gamma$  ray is found to be coincident with all the above prompt transitions and is placed above the 6957-keV, (49/2<sup>+</sup>) level based on intensity considerations. Since the ordering of the 1089- and 756-keV transitions could not be unambiguously determined from the data, the level at 10352 keV is marked as tentative. The 466-, 756-, and 1089-keV  $\gamma$  rays are clearly visible in coincidence with the 2306-keV line in Fig. 7(d).

TABLE II. Energies and intensities of  $\gamma$  rays and excitation energies and spins of initial and final states in  $^{203}\text{Tl}$  above the 6.6- $\mu\text{s}$  isomer. Statistical uncertainties on  $\gamma$ -ray energies and intensities are listed. Relative intensities have been obtained primarily from data in the prompt regime ( $\pm 40$  ns of the beam being incident on the target). The intensities in Tables I and II should be read independently of each other. Theoretical values of total conversion coefficients ( $\alpha$ ) from the BRICC tabulation [22] for the indicated multiplicities are noted where relevant. Predominant multiplicities obtained from experimental data using the procedure detailed in the text are listed; those inside parentheses are cases where the inference from experimental data is not unambiguous, while the ones in square brackets are where the assignments are based on a systematic comparison with the even isotope  $^{204}\text{Pb}$ .

$E_\gamma$ (keV)	$E_i$ (keV) $\rightarrow$ $E_f$ (keV)	$I_i^\pi \rightarrow I_f^\pi$	$I_\gamma$	$\alpha$	Mult.
211.0(1)	4441.6 $\rightarrow$ 4230.6	(35/2 <sup>-</sup> ) $\rightarrow$ (33/2 <sup>+</sup> )	68(9)	0.067	$E1$
287.7(1)	5259.6 $\rightarrow$ 4971.9	(41/2 <sup>-</sup> ) $\rightarrow$ (39/2 <sup>-</sup> )	32(2)	0.439	$M1$
312.7(2)	6957.1 $\rightarrow$ 6644.4	(49/2 <sup>+</sup> ) $\rightarrow$ (45/2 <sup>+</sup> )	17(2)	0.098	( $E2$ )
437.6(1)	6644.4 $\rightarrow$ 6206.8	(45/2 <sup>+</sup> ) $\rightarrow$ (43/2 <sup>-</sup> )	26(2)	0.012	( $E1$ )
466.0(2)	9728.8 $\rightarrow$ 9262.8	$- \rightarrow$ (55/2 <sup>-</sup> )	4(2)		-
530.3(1)	4971.9 $\rightarrow$ 4441.6	(39/2 <sup>-</sup> ) $\rightarrow$ (35/2 <sup>-</sup> )	66(4)		[ $E2$ ]
755.6(3)	11107.3 $\rightarrow$ 10351.7	$- \rightarrow -$	3(1)		-
947.2(2)	6206.8 $\rightarrow$ 5259.6	(43/2 <sup>-</sup> ) $\rightarrow$ (41/2 <sup>-</sup> )	31(3)		[ $M1$ ]
965.2(2)	4230.6 $\rightarrow$ 3265.6	(33/2 <sup>+</sup> ) $\rightarrow$ (29/2 <sup>+</sup> )	100(16)		[ $E2$ ]
1088.9(3)	10351.7 $\rightarrow$ 9262.8	$- \rightarrow$ (55/2 <sup>-</sup> )	5(2)		-
2305.7(5)	9262.8 $\rightarrow$ 6957.1	(55/2 <sup>-</sup> ) $\rightarrow$ (49/2 <sup>+</sup> )	11(3)		[ $E3$ ]

An illustrative example of the determination of multiplicity of some of the transitions above the (29/2<sup>+</sup>) isomeric level by gating on the higher-lying 2306-keV  $\gamma$  ray is given below for the 288-keV transition deexciting the 5260-keV level and feeding the 4972-keV state (Fig. 1). It may be noted that, though the 2306-keV  $\gamma$  ray has a lower intensity, and the efficiency of its detection is significantly lesser compared to lower-energy transitions, just a single gate on this transition provides a clean spectrum, owing to the absence of adjacent  $\gamma$  rays and the very low background in this region. Further, this single-gated spectrum has higher statistics than a comparable double-gated one; therefore, the uncertainties on the obtained

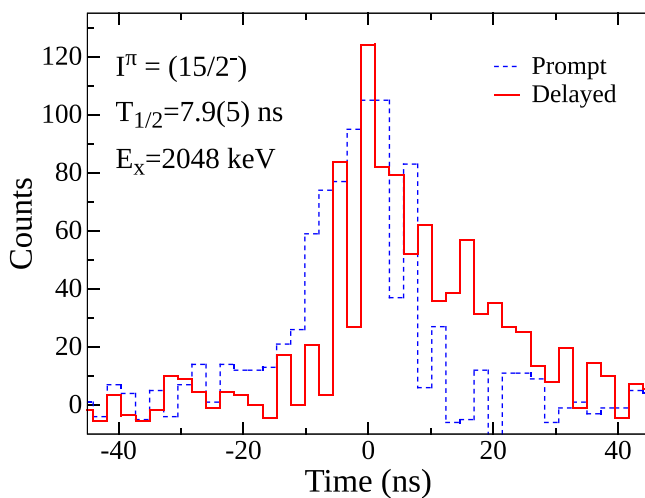


FIG. 5. Half-life of the  $I^\pi = (15/2^-)$  level measured using the centroid-shift method. The time difference between the 588- and 350-keV transitions, below and above this state, respectively, is displayed in red (solid line), while that of two prompt  $\gamma$  rays with similar energies is shown in blue (dashed line). A value of  $T_{1/2} = 7.9(5)$  ns is inferred.

intensities are, in several cases, lower than those determined by gating below the transitions of interest. The total intensity of the  $\gamma$  rays below the 2306-keV line have been balanced with that of the 965-keV one, immediately above the (29/2<sup>+</sup>) isomer (Fig. 1). Owing to its high energy, the theoretical conversion coefficient of the 965-keV transition is less than or equal to a few percentages for all reasonably possible multiplicities [22]. Therefore, its total intensity is approximately equal to its  $\gamma$ -ray intensity. In the spectrum obtained with a gate on the 2306-keV transition, the  $\gamma$ -ray intensities obtained for the 965-, 288-, 211-, and 438-keV transitions are 100(5), 71(4), 91(6), and 101(3), respectively. The total intensity of the 288-keV transition with the assumption of the following different multiplicities would be (a)  $M1$ : 102(6); (b)  $E1$ : 73(4); (c)  $E2$ : 80(5); and (d)  $M2$ : 192(11). Clearly, only  $M1$  multiplicity for the 288-keV transition would be consistent

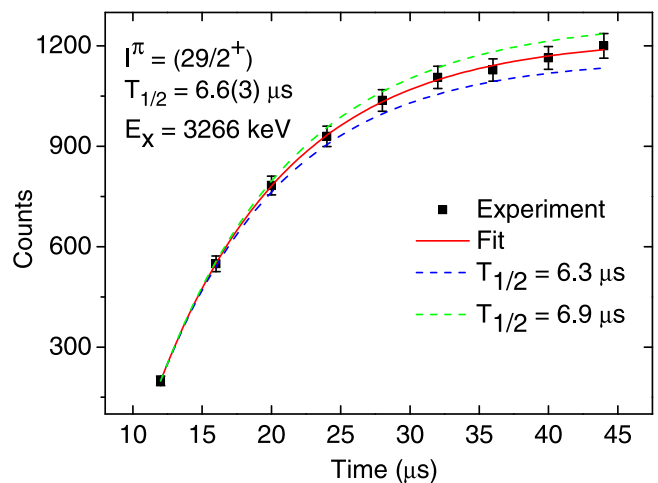


FIG. 6. Variation with time of the cumulative intensity of  $\gamma$  rays placed below the long-lived,  $\mu\text{s}$  isomeric state. A half-life of 6.6(3)  $\mu\text{s}$  is deduced for the (29/2<sup>+</sup>) state at 3266 keV.

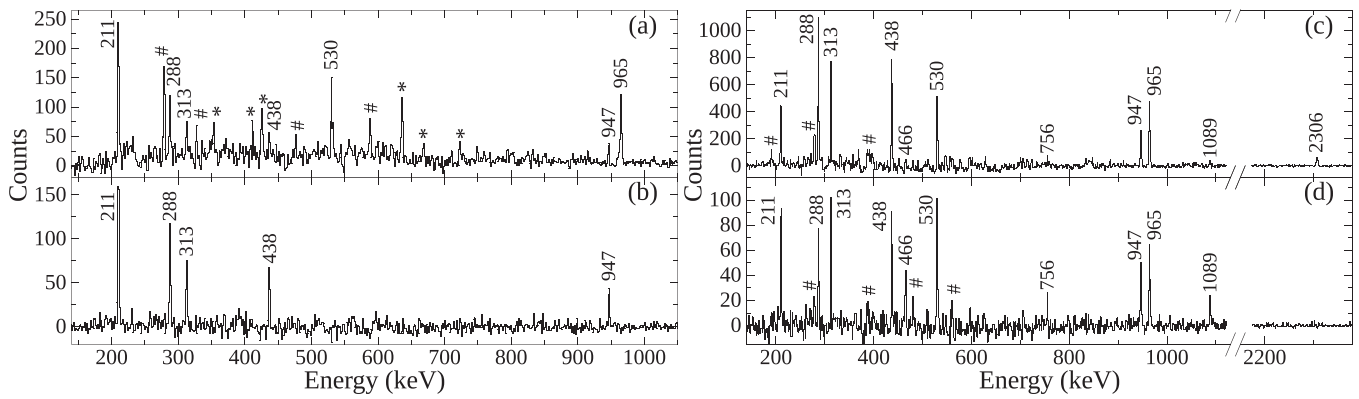


FIG. 7. (a) Spectrum measured during the beam pulse and in delayed (50-650 ns) coincidence with the 232-, 265-, 328-, 533-, 588-, and 795-keV transitions, all placed below the isomeric ( $29/2^+$ ) state at 3266 keV. Prompt  $\gamma$  rays, feeding the  $\mu$ s isomer, observed in coincidence with these delayed transitions, are displayed. The hash marks indicate intense transitions deexciting the isomer while the asterisks denote known contaminant  $\gamma$  rays from other reaction channels. (b) Prompt coincidence spectrum with gates on the 530- and 965-keV  $\gamma$  rays. (c) Prompt coincidence spectrum obtained by summing gates on two intense  $\gamma$  rays above the  $\mu$ s isomer and below the ( $49/2^+$ ) level at 6957 keV. (d) Summed coincidence spectrum with simultaneous gates on two transitions above the  $\mu$ s isomer, with one of them being the 2306-keV  $\gamma$  ray. The binning in panels (a) and (b) is 1.33 keV/channel and that in (c) and (d) is 2 keV/channel.

with intensity balance considerations. The total intensity of the 211-keV transition with the assumption of the following different multiplicities would be (a)  $E1$ : 97(6); (b)  $M1$ : 185(12); (c)  $E2$ : 122(8); and (d)  $M2$ : 533(35). Clearly, only  $E1$  multiplicity for the 211-keV transition would be consistent with intensity balance considerations. The total intensity of the 438-keV transition with the assumption of the following different multiplicities would be (a)  $E1$ : 102(3); (b)  $M1$ : 115(3); (c)  $E2$ : 105(3); and (d)  $M2$ : 145(5). While  $E1$  multiplicity for the 438-keV transition appears more likely from intensity balance considerations,  $E2$  character is not excluded by the data. A comparison with the structure of the isotone,  $^{204}\text{Pb}$  [28], supports the tentative assignment of  $E1$  character

for the 438-keV transition. The multiplicities for these and other transitions, above the ( $29/2^+$ ), 6.6- $\mu$ s isomer, obtained from the data, or from systematics, are listed in Table II.

The presence of three isomers above the  $I^\pi = (29/2^+)$  state (Fig. 1) with half-lives in the range of a few nanoseconds is deduced from an inspection of time differences of  $\gamma$  rays between the ( $29/2^+$ ) and ( $49/2^+$ ) levels at 3266 and 6957 keV, respectively (Fig. 8), and the following values have been obtained:

- (1)  $E_x = 4442$  keV,  $I^\pi = (35/2^-)$ ,  $T_{1/2} = 4.0(5)$  ns
- (2)  $E_x = 4972$  keV,  $I^\pi = (39/2^-)$ ,  $T_{1/2} = 1.9(2)$  ns
- (3)  $E_x = 6957$  keV,  $I^\pi = (49/2^+)$ ,  $T_{1/2} = 3.4(4)$  ns

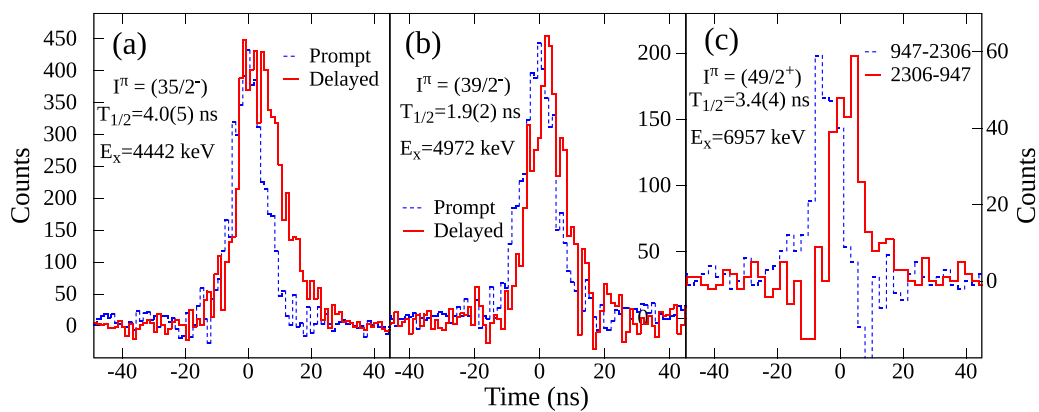


FIG. 8. Half-lives of the  $I^\pi = (35/2^-)$ , ( $39/2^-$ ), and ( $49/2^+$ ) levels at 4442, 4972, and 6957 keV, respectively, determined using the centroid-shift method. In panels (a) and (b), the histogram in red (solid line) indicates the time difference of  $\gamma$  rays below and above the relevant states while the one in blue (dashed line) corresponds to that of prompt transitions with similar energy. Values of  $T_{1/2} = 4.0(5)$  ns and 1.9(2) ns are determined for the ( $35/2^-$ ) and ( $39/2^-$ ) levels at 4442 and 4972 keV, respectively, based on the observed centroid shifts. In panel (c), the time difference between the 947- and 2306-keV  $\gamma$  rays and vice versa are compared which is equal to twice the mean life of the  $I^\pi = (49/2^+)$  level at 6957 keV, leading to a value of  $T_{1/2} = 3.4(4)$  ns for this state.

## IV. DISCUSSION

### A. Isomeric states and configurations

The high-spin isomers in Tl isotopes can be understood as resulting from the coupling of the  $h_{11/2}$  proton hole to specific neutron configurations in the corresponding Pb isotones with, in particular, a major contribution from neutrons occupying the  $i_{13/2}$  subshell. The low-lying two-neutron-hole configurations in even- $A$  Pb isotopes are the  $[\nu(i_{13/2})^{-1} \otimes \nu(p_{1/2})^{-1}]_7^-$ ,  $[\nu(i_{13/2})^{-1} \otimes \nu(f_{5/2})^{-1}]_9^-$  and  $[\nu(i_{13/2})^{-2}]_{12}^+$  ones leading to the realization of isomeric  $I^\pi = 7^-, 9^-$ , and  $12^+$  states [28,29]. The corresponding states in odd- $A$  Tl isotones have the configurations  $\pi h_{11/2}^{-1} \otimes \nu^{-2}(7^-)$ ,  $\pi h_{11/2}^{-1} \otimes \nu^{-2}(9^-)$ , and  $\pi h_{11/2}^{-1} \otimes \nu^{-2}(12^+)$  leading to  $I^\pi = 25/2^+, 29/2^+$ , and  $35/2^-$  levels. It may be noted that the  $I^\pi = (29/2^+)$  state in  $^{203}\text{Tl}$  is the analog of the isomeric  $9^-$  levels in Pb isotopes [28–30]. The  $25/2^+$  and  $35/2^-$  states in  $^{205}\text{Tl}$  have been determined to be isomeric with  $T_{1/2} = 2.6 \mu\text{s}$  and  $T_{1/2} = 235 \text{ ns}$ , respectively [2]. Since the  $29/2^+ \rightarrow 25/2^+ E2$  transition in  $^{205}\text{Tl}$  has an energy of 328 keV, the decay of the  $29/2^+$  level has been found to be prompt [2]. Analogous isomeric levels have not been identified in lighter, odd- $A$  Tl isotopes with mass  $A \leq 199$ , most likely due to the underlying weak oblate deformation and resultant collective structures. In  $^{201}\text{Tl}$ , the presence of such isomeric states has not yet been established [31]; however, their existence cannot be ruled out. In  $^{203}\text{Tl}$ , under discussion here, the observed long-lived decay, with  $T_{1/2} = 6.6(3) \mu\text{s}$ , is associated with the  $29/2^+$  level. The excitation energies of the  $25/2^+$  levels in  $^{203,205}\text{Tl}$  are quite similar (3260 and 3291 keV, respectively). This may be understood as follows: The  $\pi h_{11/2}$  and  $\nu p_{1/2}$  quasiparticle energies in the two isotopes are quite similar; however, the  $\nu i_{13/2}$  one in  $^{203}\text{Tl}$  is lower by virtue of its relative proximity to the neutron Fermi level in comparison to  $^{205}\text{Tl}$ . This difference is compensated to a significant extent by the fact that the neutron pair-gap energy in  $^{205}\text{Tl}$  is lower than that in  $^{203}\text{Tl}$  [32], leading to the observed similarity of the excitation energies of the  $25/2^+$  levels in the two isotopes. The small separation (6 keV) between the  $25/2^+$  and  $29/2^+$  levels in  $^{203}\text{Tl}$  is mirrored in  $^{204}\text{Pb}$ , where the  $7^-$  and  $9^-$  levels are 79 keV apart [28]. An important difference is that the  $9^-$  state is lower in  $^{204}\text{Pb}$  in contrast to the  $25/2^+$  level in  $^{203}\text{Tl}$ . The identification of the closely-spaced pair of levels with  $I^\pi = 25/2^+$  and  $29/2^+$  in  $^{203}\text{Tl}$  thus provides insight into the difference of the magnitude of residual interactions of the  $h_{11/2}$  proton with the respective two-neutron-hole configurations in  $^{204}\text{Pb}$ . The transition rates for the  $I^\pi = 29/2^+$  isomeric decays are consistent with Weisskopf estimates and those in neighboring nuclei, e.g.,  $B(E3)$  (334 keV) = 5.8 W.u. The unhindered  $E3$  decay likely implies a configuration change from  $\pi h_{11/2}^{-1} \otimes \nu^{-2}(9^-)$  to  $\pi d_{5/2}^{-1} \otimes \nu^{-2}(9^-)$  for the  $29/2^+ \rightarrow 23/2^-$  transition in  $^{203}\text{Tl}$ .

In  $^{203}\text{Tl}$ , there are four neutron holes in contrast to only two in  $^{205}\text{Tl}$ . Consequently, levels with one-proton and four-neutron-hole configurations are possible in  $^{203}\text{Tl}$ , unlike in  $^{205}\text{Tl}$  where only two neutron holes are present. As a result, in  $^{205}\text{Tl}$ , there is no intervening level between the  $29/2^+$  and

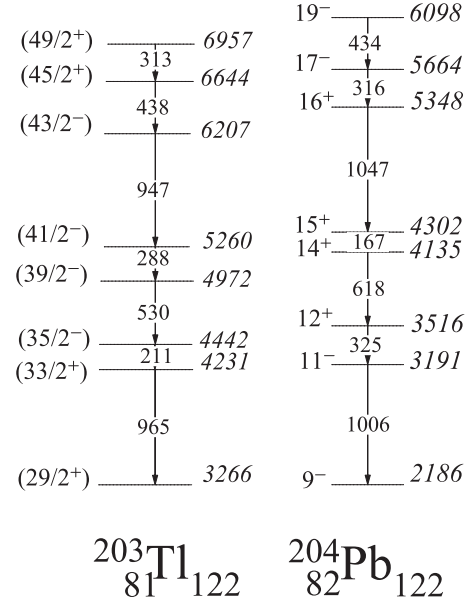


FIG. 9. Comparison of the level structure above the analogous  $29/2^+$  and  $9^-$  isomeric states in  $^{203}\text{Tl}$  and  $^{204}\text{Pb}$ , respectively.

$35/2^-$  states, and the  $35/2^-$  state decays by a 1217-keV,  $E3$  transition and is characterized by a half-life of  $T_{1/2} = 235(10) \text{ ns}$  [2]. The  $I^\pi = 35/2^-$  state represents the maximum spin achievable from a three-nucleon-hole configuration, resulting from one  $h_{11/2}$  proton and two  $i_{13/2}$  neutrons. This state at 4442 keV is found to be isomeric in  $^{203}\text{Tl}$  as well, with  $T_{1/2} = 4.0(5) \text{ ns}$ . It decays to the 4231-keV,  $(33/2^+)$  level which has a five-nucleon-hole configuration, with likely mixed character comprising  $\pi h_{11/2}^{-1} \otimes \nu(i_{13/2}^{-1}, f_{5/2}^{-2}, p_{1/2}^{-1})$  and  $\pi h_{11/2}^{-1} \otimes \nu(i_{13/2}^{-1}, f_{5/2}^{-1}, p_{3/2}^{-1}, p_{1/2}^{-1})$  configurations. All the levels above the 4442-keV,  $(35/2^-)$  state must have configurations involving five or more nucleons. The observed isomerism of the 4972-keV,  $(39/2^-)$  state may be qualitatively understood in terms of the hindrance induced by the change of two neutrons in the configurations of the initial and final states in each of these cases. The 6957-keV,  $I^\pi = 49/2^+$  state most likely results from the coupling of  $\pi h_{11/2}^{-1} \otimes \nu^{-4}(19^-)$ , with the neutron configuration corresponding to the relevant level established in the  $^{204}\text{Pb}$  isotone [28]. A comparison of the level structure of  $^{203}\text{Tl}$  above the  $29/2^+$  state and the most intense cascade above the analogous  $9^-$  level in  $^{204}\text{Pb}$  is displayed in Fig. 9. It may be noted that while the placements and multipolarities of most of the transitions in  $^{203}\text{Tl}$  have been obtained from the experimental data, in a few cases, the multipolarities are based on a comparison with the ones in  $^{204}\text{Pb}$  [28].

### B. “Empirical” calculations

“Empirical” calculations, based on near-neighbor systematics, have been performed to estimate the energies of isomeric states. For this purpose, the average of 1-quasineutron energies from neighboring, odd- $A$  Pb isotopes ( $^{203,205}\text{Pb}$ ), and 1-quasiproton energies derived from the corresponding excited levels in  $^{203}\text{Tl}$ , were used [26,27,33]. The neutron

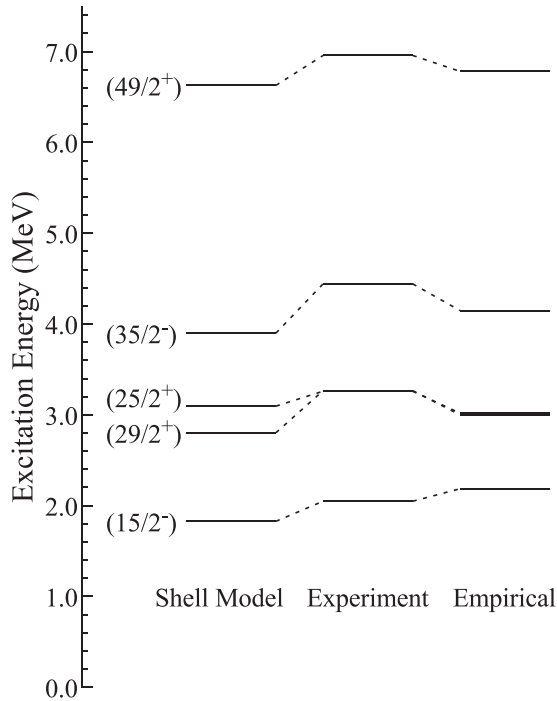


FIG. 10. Excitation energies of selected states in  $^{203}\text{Tl}$  obtained from experiment and their comparison with empirical and shell-model calculations discussed in the text. The calculated transition rates are listed in the text.

pair-gap energies were obtained using the five-point formula involving odd-even mass differences [32]. To calculate the energies of states with multinucleon configurations, the relevant 1-quasiparticle energies were summed with the pair-gap energy, and appropriate corrections were incorporated for the residual interactions. The magnitude of residual interactions was determined from isomeric configurations in neighboring Tl and Pb isotopes and the following values were obtained:  $15/2^-$  (119 keV):  $\pi h_{11/2}^{-1} \otimes \nu(f_{5/2}^{-1}, p_{1/2}^{-1})$ ;  $25/2^+$  (204 keV):  $\pi h_{11/2}^{-1} \otimes \nu(i_{13/2}^{-1}, p_{1/2}^{-1})$ ;  $29/2^+$  (160 keV):  $\pi h_{11/2}^{-1} \otimes \nu(i_{13/2}^{-1}, f_{5/2}^{-1})$ ;  $35/2^-$  (13 keV):  $\pi h_{11/2}^{-1} \otimes \nu(i_{13/2}^{-2})$ . The calculated energies of the abovementioned states and a comparison with experimental values is displayed in Fig. 10. Sufficient experimental data are not available to determine the residual interactions for the five-nucleon configuration responsible for the  $49/2^+$  [ $\pi h_{11/2}^{-1} \otimes \nu(i_{13/2}^{-3}, f_{5/2}^{-1})$ ] state. Therefore, the energy for this state has been obtained by summing the experimental value of the  $29/2^+$  state in  $^{203}\text{Tl}$  with that of the

$\nu i_{13/2}^{-2}$ ,  $12^+$  level in  $^{204}\text{Pb}$  [28]. While the empirical calculations underestimate the experimental energies in most cases, there is fair agreement between the two, with the deviations being less than 300 keV for all states.

### C. Shell-model calculations

Shell-model calculations have been performed for  $^{203}\text{Tl}$  employing the KHH7B [34] effective interaction. Since proton excitations across the  $Z = 82$  shell gap and neutron ones across the  $N = 126$  one were not allowed, the active orbitals in the shell-model calculations are  $d_{5/2}$ ,  $h_{11/2}$ ,  $d_{3/2}$ , and  $s_{1/2}$  for protons and  $i_{13/2}$ ,  $p_{3/2}$ ,  $f_{5/2}$ , and  $p_{1/2}$  for neutrons. The shell-model code Oxbash [35] was used for the diagonalization of the matrices of interest. The deviations of the predicted energies from the experimental values are about 200–300 keV for the  $15/2^-$  and  $49/2^+$  states and  $\approx 500$  keV for the  $29/2^+$  and  $35/2^-$  levels. The  $29/2^+$  state is calculated to be lower in energy than the  $25/2^+$  level, unlike what is displayed by the data (Fig. 10). A comparison of the excitation energies from experiment and those from both empirical and shell-model calculations is presented in Table III, along with the primary underlying configurations. The transition rates for the 6-keV  $E2$  and 334-keV  $E3$  transitions deexciting the  $29/2^+$  state at 3266 keV are calculated to be 7.1 and 0.6 W.u., respectively. The significant disagreement between the experimental and calculated energies for the  $29/2^+$  and  $35/2^-$  states, and transition rates for decay of the former, indicate the need for improving the interactions used in the shell-model calculations.

### D. Octupole core excitations

The level with  $E_x = 9263$  keV is suggested to have  $I^\pi = (55/2^-)$  because it is interpreted as the octupole excitation of the  $^{208}\text{Pb}$  core built on the  $\pi h_{11/2}^{-1} \otimes \nu(i_{13/2}^{-3}, f_{5/2}^{-1})$ ,  $I^\pi = 49/2^+$  configuration. The energy of the  $55/2^- \rightarrow 49/2^+$  transition (2306 keV) is consistent with this interpretation, as described below. It is worth noting that similar transitions with energies 2207 and 2256 keV are observed above the four- and three-nucleon-hole states in  $^{204}\text{Tl}$  and  $^{205}\text{Tl}$ , respectively [2,3]. Following the prescription outlined previously [2,3,36], the expected transition energy for the  $E3$  excitation built on the five-nucleon hole,  $49/2^+$  state can be estimated. While the unperturbed energy of the  $E3$  excitation in  $^{208}\text{Pb}$  would be 2615 keV, energy shifts would result from the coupling to configurations involving multiple nucleons. These can be expressed as the sum of energy shifts corresponding to the

TABLE III. Energies and spins of isomeric levels in  $^{203}\text{Tl}$  from experiment and empirical as well as shell-model calculations (see text for details). The predicted (main) partitions are also listed.

$I_i^\pi$	$T_{1/2}$	Configuration	Partition (%)	$E_{\text{exp}}$ (keV)	$E_{\text{emp}}$ (keV)	$E_{\text{SM}}$ (keV)
$15/2^-$	7.9(5) ns	$\pi s_{1/2}^{-1} \nu(p_{1/2}^{-1}, i_{13/2}^{-1})$	32	2048	2185	1827
$29/2^+$	6.6(3) $\mu\text{s}$	$\pi h_{11/2}^{-1} \nu(f_{5/2}^{-1}, i_{13/2}^{-1})$	60	3266	2999	2803
$35/2^-$	4.0(5) ns	$\pi h_{11/2}^{-1} \nu i_{13/2}^{-2}$	49	4442	4148	3899
$49/2^+$	3.4(4) ns	$\pi h_{11/2}^{-1} \nu(f_{5/2}^{-1}, i_{13/2}^{-3})$	100	6957	6782	6627

individual constituents of such a configuration. For instance, as described previously [3,36], energy shifts of  $\Delta E = -150$  keV and  $+40$  keV are obtained based on the following transitions:  $17/2^+ \rightarrow 11/2^-$  (2465 keV) in  $^{207}\text{Tl}$  and  $11/2^+ \rightarrow 5/2^-$  (2655 keV) in  $^{207}\text{Pb}$ , respectively. These transitions represent the stretched  $E3$  excitations built on the  $\pi h_{11/2}^{-1}$  and  $\nu f_{5/2}^{-1}$  states in  $^{207}\text{Tl}$  and  $^{207}\text{Pb}$ , respectively. For the  $\nu i_{13/2}^{-3}$  configuration, an energy shift of  $-262$  keV has been estimated [3] since the  $E3$  excitation built on the  $\nu i_{13/2}^{-3}$ ,  $I^\pi = 33/2^+$  state has not been identified yet. Thus, for the  $\pi h_{11/2}^{-1} \otimes \nu(i_{13/2}^{-3}, f_{5/2}^{-1})$  configuration, an addition of the above mentioned energy shifts yields a value of  $-372$  keV, implying an estimated  $55/2^- \rightarrow 49/2^+$ , 2243-keV transition energy. This estimated value is lower than the observed one by only 63 keV. The situation is similar to that observed for the  $\pi h_{11/2}^{-1} \otimes \nu(i_{13/2}^{-2}, f_{5/2}^{-1})$ ,  $I^\pi = 20^+$  configuration in  $^{204}\text{Tl}$  [3] where the estimated value is 61 keV lower than the experimental one. It is worth noting that even better agreement (within several keV) between estimated and experimental values is seen for the  $22^+$  state in  $^{204}\text{Tl}$  [3] and  $35/2^-$  level in  $^{205}\text{Tl}$  [2], e.g., excitations involving high- $j$  orbitals only. This likely suggests an underestimation of the magnitude of the repulsive interaction of the stretched- $E3$  excitation with the  $f_{5/2}$  neutron hole. On the other hand, the reasonable agreement between estimated and experimental values appears to validate the assignment of the 2306-keV transition in  $^{203}\text{Tl}$  as the octupole core excitation built on the  $49/2^+$  state at 6957 keV.

## V. SUMMARY

The level structure of  $^{203}\text{Tl}$  has been considerably expanded and is now established up to high spin with the inclusion of 25 new transitions, five isomeric states, and octupole core excitations built on a five-nucleon-hole configuration. Isomeric states with  $I^\pi = (15/2^-)$ ,  $(35/2^-)$ ,  $(39/2^-)$ , and  $(49/2^+)$  at 2048, 4442, 4972, and 6957 keV, respectively, with corresponding half-lives of  $T_{1/2} = 7.9(5)$  ns, 4.0(5) ns,

1.9(2) ns, and 3.4(4) ns, have been identified. The half-life of the previously determined long-lived decay is determined to be  $6.6(3)$   $\mu\text{s}$ , in comparison to the earlier reported value of  $7.7(5)$   $\mu\text{s}$ , and is associated with the  $I^\pi = (29/2^+)$  state at 3266 keV. The structure of the levels fed by this long-lived decay is significantly modified. The  $\gamma$  rays feeding the 6.6  $\mu\text{s}$  isomer have been identified through delayed-prompt coincidence measurements. Of particular note is the observation of octupole core excitations built on a five-nucleon hole configuration. ‘‘Empirical’’ calculations, based on near-neighbor systematics, are able to satisfactorily reproduce key states in the experimental level scheme, while those using the shell model appear to significantly underestimate the state energies in two instances. These results contribute valuable information towards improving the understanding of nuclear structure in the vicinity of the heaviest doubly magic nucleus,  $^{208}\text{Pb}$ .

## ACKNOWLEDGMENTS

The authors thank I. Ahmad, J. P. Greene, T. L. Khoo, A. J. Knox, C. J. Lister, D. Peterson, U. Shirwadkar, X. Wang, and C. M. Wilson for assistance during the experiment. V.B. acknowledges assistance under the INSPIRE fellowship of the Department of Science and Technology, Government of India. S.K.T. acknowledges support from the University Grants Commission, India, under the Faculty Recharge Programme. S.G.W. acknowledges support from the DST-INSPIRE Ph.D. Fellowship of the Department of Science and Technology, Government of India (Fellowship No. IF150098). P.C.S. acknowledges a research grant from the Science and Engineering Research Board (India), CRG/2019/000556. This work is supported by the U.S. Department of Energy, Office of Science, Office of Nuclear Physics, under Awards No. DE-FG02-94ER40848 and No. DE-FG02-94ER40834 (UML), No. DE-FG02-97ER41041 (UNC) and No. DE-FG02-97ER41033 (TUNL), and Contract No. DE-AC02-06CH11357 (ANL). The research described here utilized resources of the ATLAS facility at ANL, which is a DOE Office of Science user facility.

- 
- [1] O. Häusser, J. R. Beene, T. K. Alexander, A. B. McDonald, and T. Faestermann, *Phys. Lett. B* **64**, 273 (1976).
- [2] J. Wrzesiński, R. Broda, B. Fornal, W. Królas, T. Pawłat, M. P. Carpenter, R. V. F. Janssens, D. Seweryniak, S. Lunardi, C. A. Ur *et al.*, *Eur. Phys. J. A* **20**, 57 (2004).
- [3] R. Broda, K. H. Maier, B. Fornal, J. Wrzesiński, B. Szipak, M. P. Carpenter, R. V. F. Janssens, W. Królas, T. Pawłat, and S. Zhu, *Phys. Rev. C* **84**, 014330 (2011).
- [4] B. Szipak, K. H. Maier, A. S. Smolkowska, B. Fornal, R. Broda, M. P. Carpenter, N. Cieplicka, R. V. F. Janssens, W. Krolas, T. Pawłat, J. Wrzesiński, and S. Zhu, *Phys. Rev. C* **83**, 064315 (2011).
- [5] J. Wrzesiński, G. J. Lane, K. H. Maier, R. V. F. Janssens, G. D. Dracoulis, R. Broda, A. P. Byrne, M. P. Carpenter, R. M. Clark, M. Cromaz, B. Fornal, T. Lauritsen, A. O. Macchiavelli, M. Rejmund, B. Szipak, K. Vetter, and S. Zhu, *Phys. Rev. C* **92**, 044327 (2015).
- [6] A. J. Kreiner, M. Fenzl, S. Lunardi, and M. A. J. Mariscotti, *Nucl. Phys. A* **282**, 243 (1977).
- [7] E. A. Lawrie, P. A. Vymers, Ch. Vieu, J. J. Lawrie, C. Schück, R. A. Bark, R. Lindsay, G. K. Mabala, S. M. Maliage, P. L. Masiteng *et al.*, *Eur. Phys. J. A* **45**, 39 (2010).
- [8] S. G. Wahid, S. K. Tandel, Saket Suman, M. Hemalatha, Anurag Patel, Poulomi Roy, A. Y. Deo, Pragati, P. C. Srivastava, B. Bhoy, S. S. Bhattacharjee, R. P. Singh, S. Muralithar, P. Chowdhury, R. V. F. Janssens, M. P. Carpenter, T. L. Khoo, F. G. Kondev, T. Lauritsen, C. J. Lister, D. Seweryniak, S. Zhu, S. Rai, and A. Sharma, *Phys. Rev. C* **102**, 024329 (2020).
- [9] M. G. Slocombe, J. O. Newton, and G. D. Dracoulis, *Nucl. Phys. A* **275**, 166 (1977).
- [10] A. J. Kreiner, M. A. J. Mariscotti, C. Baktash, E. der Mateosian, and P. Thieberger, *Phys. Rev. C* **23**, 748 (1981).
- [11] P. Roy, S. K. Tandel, S. Suman, P. Chowdhury, R. V. F. Janssens, M. P. Carpenter, T. L. Khoo, F. G. Kondev, T. Lauritsen, C. J.

- Lister, D. Seweryniak, and S. Zhu, *Phys. Rev. C* **100**, 024320 (2019).
- [12] M. Pfützner, P. Armbruster, T. Baumann, J. Benlliure, M. Bernas, W. N. Catford, D. Cortina-Gil, J. M. Daugas, H. Geissel, M. Górska *et al.*, *Phys. Lett. B* **444**, 32 (1998).
- [13] S. J. Steer, Zs. Podolyák, S. Pietri, M. Górska, P. H. Regan, D. Rudolph, E. Werner-Malento, A. B. Garnsworthy, R. Hoischen, J. Gerl *et al.*, *Phys. Rev. C* **78**, 061302 (2008).
- [14] Zs. Podolyák, S. J. Steer, S. Pietri, M. Górska, P. H. Regan, D. Rudolph, A. B. Garnsworthy, R. Hoischen, J. Gerl, H. J. Wollersheim *et al.*, *Eur. Phys. J. A* **42**, 489 (2009).
- [15] S. J. Steer, Zs. Podolyák, S. Pietri, M. Górska, H. Grawe, K. H. Maier, P. H. Regan, D. Rudolph, A. B. Garnsworthy, R. Hoischen *et al.*, *Phys. Rev. C* **84**, 044313 (2011).
- [16] M. Bowry, Zs. Podolyák, S. Pietri, J. Kurcewicz, M. Bunce, P. H. Regan, F. Farinon, H. Geissel, C. Nociforo, A. Prochazka *et al.*, *Phys. Rev. C* **88**, 024611 (2013).
- [17] N. Lalović, D. Rudolph, Zs. Podolyák, L. G. Sarmiento, E. C. Simpson, T. Alexander, M. L. Cortiés, J. Gerl, P. Golubev, F. Ameil *et al.*, *J. Phys. G (Lond.)* **45**, 035105 (2018).
- [18] I.-Y. Lee, *Nucl. Phys. A* **520**, c641 (1990).
- [19] R. V. F. Janssens and F. S. Stephens, *Nucl. Phys. News* **6**, 9 (1996).
- [20] H.-Q. Jin, TSCAN and related programs, A package to perform tape scanning and to manipulate matrices, RUTGERS-ORNL-UTK (1997).
- [21] D. C. Radford, *Nucl. Instrum. Methods A* **361**, 297 (1995).
- [22] T. Kibedi, T. W. Burrows, M. B. Trzhaskovskaya, P. M. Davidson, C. W. Nestor, Jr., *Nucl. Instrum. Methods A* **589**, 202 (2008).
- [23] S. K. Tandel, S. G. Wahid, P. Chowdhury, R. V. F. Janssens, M. P. Carpenter, T. L. Khoo, F. G. Kondev, T. Lauritsen, C. J. Lister, D. Seweryniak *et al.*, *Phys. Lett. B* **750**, 225 (2015).
- [24] S. K. Tandel, P. Chowdhury, F. G. Kondev, R. V. F. Janssens, T. L. Khoo, M. P. Carpenter, T. Lauritsen, C. J. Lister, D. Seweryniak, S. Zhu, A. Deacon, S. J. Freeman, N. J. Hammond, G. D. Jones, E. F. Moore, and J. F. Smith, *Phys. Rev. C* **94**, 064304 (2016).
- [25] S. G. Wahid, S. K. Tandel, P. Chowdhury, R. V. F. Janssens, M. P. Carpenter, T. L. Khoo, F. G. Kondev, T. Lauritsen, C. J. Lister, D. Seweryniak, and S. Zhu, *Phys. Rev. C* **92**, 054323 (2015).
- [26] F. G. Kondev, *Nucl. Data Sheets* **177**, 509 (2021).
- [27] F. G. Kondev, *Nucl. Data Sheets* **166**, 1 (2020).
- [28] C. G. Lindén, I. Bergström, J. Blomqvist, and C. Roulet, *Z. Phys. A* **284**, 217 (1978).
- [29] R. Lutter, O. Häusser, D. J. Donahue, R. L. Hershberger, F. Riess, H. Bohn, T. Faestermann, F. v. Feilitzsch, and K. E. G. Löbner, *Nucl. Phys. A* **229**, 230 (1974).
- [30] U. Rosengård, P. Carlè, A. Källberg, L. O. Norlin, K. G. Rensfelt, H. C. Jain, B. Fant, and T. Weckström, *Nucl. Phys. A* **482**, 573 (1988).
- [31] S. Das Gupta, S. Bhattacharyya, H. Pai, G. Mukherjee, S. Bhattacharya, R. Palit, A. Shrivastava, A. Chatterjee, S. Chanda, V. Nanal, S. K. Pandit, S. Saha, J. Sethi, and S. Thakur, *Phys. Rev. C* **88**, 044328 (2013).
- [32] P. Möller and J. R. Nix, *Nucl. Phys. A* **536**, 20 (1992).
- [33] F. G. Kondev, *Nucl. Data Sheets* **108**, 365 (2007).
- [34] G. H. Herling and T. T. S. Kuo, *Nucl. Phys. A* **181**, 113 (1972).
- [35] B. A. Brown, Oxbash for Windows, MSU-NSCL Report 1289, 2004.
- [36] M. Kadi, P. E. Garrett, Minfang Yeh, S. W. Yates, T. Belgia, A. M. Oros-Peusquens, and K. Heyde, *Phys. Rev. C* **61**, 034307 (2000).